International Journal of Adhesion & Adhesives 130 (2024) 103617

Contents lists available at ScienceDirect

International Journal of Adhesion and Adhesives

journal homepage: www.elsevier.com/locate/ijadhadh

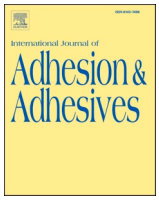

Processing understanding, mechanical durability and hygrothermal stability of PC/AA6061 hybrid joints produced via injection overmolding

G.H.M. Oliveira [a,b,*], S.T. Amancio-Filho [b], L.B. Canto [a,**]

[a] Department of Materials Engineering (DEMa), Graduate Program in Materials Science and Engineering (PPGCEM), Federal University of Sao Carlos (UFSCar), Sao Carlos, SP, Brazil
[b] Institute of Materials Science, Joining and Forming, BMK Endowed Professorship for Aviation, Graz University of Technology (TU Graz), Graz, Austria

ARTICLE INFO

Keywords:
Injection molding
Direct joining
Polymer-metal
Fatigue
Aging

ABSTRACT

In the present study, single-lap joints of polycarbonate (PC) and laser-textured aluminum alloy AA6061 were manufactured by injection overmolding (IOM) and characterized in terms of the microstructure, quasi-static and long-term mechanical performance and hygrothermal stability. The injection overmolding parameters were optimized through design of experiments and analysis of variance, which showed that the parameters of barrel temperature, injection speed and holding pressure positively affected the ultimate lap-shear force (ULSF). PC/AA6061 injection overmolded hybrid joints exhibited outstanding joining strength of 7.2 ± 0.5 MPa. Under fatigue cyclic loading, hybrid joints produced with optimized IOM processing conditions showed a fatigue life of 35 % ULSF at 10^6 cycles, demonstrating excellent mechanical durability. Moreover, PC/AA6061 injection overmolded hybrid joints showed good hygrothermal stability, with no significant variations in joining strength after aging in water at 80 °C for 30 days.

1. Introduction

Engineering polymers have gained ground in structural applications in the automotive and aeronautic sectors [1]. On the one hand, this pattern is brought by the low density, simple processing requirements, design flexibility and strong chemical resistance of engineering polymers. On the other hand, although heavier, metals have greater stiffness and strength than polymers, making them more suitable for load-bearing applications [2]. In this regard, the development of polymer-metal hybrid (PMH) structures, which can synergistically combine the capabilities of both materials and fill specific deficiencies of each class, has eased this dichotomy between choosing polymer or metal materials [3,4]. Indeed, PMH structures have been widely studied and employed in the transport industry to reduce vehicle weight, fuel/energy consumption, and CO_2 emissions [4–6]. Among the materials of great interest in the production of PMHs are polycarbonate (PC) and aluminum alloys. These materials are widely used as adjacent components in vehicles [7]. PC is frequently employed for lenses and can even replace vehicle windshields. AA6061 is one of the most commonly used aluminum alloys in automotive components, including vehicle bodies and engine parts [8].

Injection overmolding offers great advantages in manufacturing structures, as it allows molding polymer components and joining with the metal part in a single step through a fast, precise, efficient and automated process [9,10]. In the direct-adhesion injection overmolding method, a metal insert or profile is surface treated to produce micro- or nano-scale features that, when filled with the molded polymer, provide adhesive forces between the polymer and metal parts and thus lead to strong joints [11,12]. PMH joints produced via injection overmolding with laser surface textured metals have been the subject of several studies [13–20]. The laser ablates a metal layer to create microcavities on the metal surface, and the resulting pattern can be controlled by the scan configuration and proper laser parameter selection [17–19]. These studies have focused on evaluating the effects of different materials, metal surface patterns, and occasionally processing conditions on the lap-shear strength of joints. Gebauer et al. [18] used continuous wave (cw) laser to structure the metal surface in single-lap joints of polyamide 66 (PA66) and 6082-T6 aluminum alloy, producing trench patterns with hatch distances of 150 μm and depth of 158 ± 17 μm. The injection overmolding parameters were kept constant (barrel temperature, T_b of

* Corresponding author. Department of Materials Engineering (DEMa), Graduate Program in Materials Science and Engineering (PPGCEM), Federal University of Sao Carlos (UFSCar), Sao Carlos, SP, Brazil.
** Corresponding author.
E-mail addresses: marcatto@tugraz.at (G.H.M. Oliveira), leonardo@ufscar.br (L.B. Canto).

https://doi.org/10.1016/j.ijadhadh.2023.103617
Received 25 August 2023; Received in revised form 9 November 2023; Accepted 28 December 2023
Available online 31 December 2023

285 °C, mold temperature, T_{md} of 80 °C and flow rate, R_f of 15 $cm^3\ s^{-1}$). Metal trenches were almost completely filled with PA66, resulting in a joining strength of 11.9 MPa. Huang et al. [19] produced periodic holes on the metal surface of glass-fiber reinforced polyamide (PA-35GF) and steel (grade 340/590 DP) single-lap joints using nanosecond pulsed laser treatment. The spacing between adjacent holes varied between 50 μm and 300 μm. The conditions for injection overmolding were kept constant (T_b of 285 °C, T_{md} of 90 °C and R_f of 12 $cm^3\ s^{-1}$). Using a line-point pattern analysis (the ratio of the hole diameter to the distance between adjacent holes), the joining strength increased with increasing surface roughness and spacing between adjacent holes, reaching a maximum of 27.8 MPa for a 1:3 line-point pattern. Zhao et al. [13] investigated the effects of packing and holding pressures as well as polymer melt temperature on the lap-shear strength of PBT-30GF/AA5052 single-lap joints. Micrometric dimples with a fixed aspect ratio (depth/diameter) of 1.5 were placed in a square pattern on metal substrates using a nanosecond pulsed laser. Two groups of molding conditions were evaluated: one with varying packing pressures from 20 MPa to 100 MPa and polymer temperatures from 220 °C to 245 °C, and other group with changing holding pressure from 0 to 50 MPa and melt temperatures from 230 °C to 245 °C, with constant packing pressure of 100 MPa. Hybrid joint strength increased with packing pressure. Only at 20 MPa packing pressure did joint strength increase significantly with increasing temperature. The authors demonstrated that the increase of packing pressure and melt temperature enhanced polymer filling into the dimples and thus, the mechanical interlocking effect. Zhao et al. [15] investigated overlap joints of amorphous polycarbonate (PC) and poly(methyl methacrylate) (PMMA) with laser-textured aluminum alloy AA5052. Holes of 50 μm in diameter, 100 μm in-depth, and spaced 60 μm apart were laser ablated into the surface of the metal. The injection speed varied between 10 mm/s and 100 mm/s, the packing pressure varied between 20 MPa and 80 MPa, while the holding pressure varied between 15 MPa and 60 MPa. The authors found that higher packing pressure and injection speed values are required for obtaining greater polymer filling into the metal holes and, thus, high shear strength. Moreover, a linear increase between polymer filling depth and ultimate lap-shear strength was observed. For a packing/holding pressure of 80/60 MPa, the shear strength increased from 7.5 MPa to 5.5 MPa at 10 mm/s to 30 MPa and 20 MPa at 100 mm/s for PC and PMMA, respectively.

This study aims to better understand injection overmolding conditions on the lap-shear strength and gain new insights into the fatigue behavior and hygrothermal stability of overlap joints between polycarbonate (PC) and laser-textured aluminum alloy 6061. Optimization of injection overmolding parameters through the design of experiments and analysis of variance based on the quasi-static lap-shear strength of joints, the behaviors of the PC/AA6061 joints under fatigue testing and hygrothermal aging are addressed.

2. Materials and methods

2.1. Materials

The polymer component was a commercial grade polycarbonate, PC (commercial grade LEXAN™ 103) with a melt flow rate of 7 g/10 min (ASTM 1238: 300 °C, 1.2 kg) supplied by SABIC Innovative Plastics, Brazil. PC is an amorphous engineering thermoplastic widely used in injection-molded parts for automotive and household appliances requiring high stiffness, strength and toughness, good dimensional stability, and optical transparency.

6 mm-thick 6061-T6 aluminum alloy rolled sheets (AA6061) produced by Alcoa, USA were used. This alloy combines good workability, relatively high mechanical strength and corrosion resistance [21] with a wide use for engineering and structural applications in boats, furniture, and automobiles.

2.2. Metal surface treatment

AA6061 metal inserts are one symmetrical side of a half-lap splice joint with dimensions shown in Fig. 1a, which were cut and machined from the rolled sheets. The recessed area of the AA6061 insert was texturized by laser to promote better adhesion with PC. A pulsed Nd-YAG laser (Trotec SpeedMarker 50, Austria) with 20 W of average power, wavelength of 1064 nm and laser spot diameter of 45 μm was used. A pattern of micron-scale grooves spaced (center to center) of 100 μm each and oriented in the direction transverse to the length axis of the AA6061 insert was produced, as shown in Fig. 1b. Additional studies (not addressed in this publication) have shown ductile failure in the PC component with the highest ULSF value of 2210 ± 55 N (+6 %) for joints produced in the optimized injection molding condition with AA6061 inserts containing deeper grooves (65 μm). Therefore, delamination failure was induced for produced specimens in this study by adjusting the laser texturing conditions of the metal surface, which produced a groove depth of slightly less than 65 μm. Laser scanning conditions were: frequency 20 kHz, laser scan speed 500 mm/s and four scans. The parameters used were selected from the laser texturing parameters surveyed in the literature and preliminary testing [17–20]. The laser was scanned line by line, back and forth, four times, resulting in grooves with a width of 45 ± 1 μm and depth of 55 ± 5 μm, as schematically shown in Fig. 1b. Metal inserts were cleaned in an ultrasonic bath with isopropyl alcohol for 10 min and at 30 °C, followed by cleaning with pressurized air before and after laser texturing. This cleaning procedure was applied to remove grease and debris that do not adhere to the textured metal surface and can act as a weak boundary layer.

2.3. Injection overmolding

PC/AA6061 joints with half-lap splice configuration (Fig. 2) were prepared using an Arburg Allrounder 270V injection molding machine (Arburg, Germany) operated in semi-automatic mode, with the metal inserts being manually positioned into the mold cavity before each molding cycle. The dimensions of the joint and overlap region were adapted from the ASTM D1002 standard - a guideline for testing the strength of adhesives for joining metals - which has been widely used for evaluating the lap-shear strength of PMHs. Fig. 3 shows a photograph of an injection overmolded PC/AA6061 hybrid joint specimen containing the sprue, runner and gate.

A 2^3-full factorial design of experiments (DoE) with one center point (CP) and five replicate specimens for each condition was used to understand and optimize the injection overmolding of PC/AA6061 joints. The injection overmolding parameter range of values was selected based on the PC processing window. Additionally, the molding conditions were chosen to yield high-strength joints, ensuring the polymer component is free from volumetric or surface defects. The DoE factors, namely, barrel temperature, injection speed and holding pressure, were varied by two levels each, as shown in Table 1. Other injection overmolding conditions were kept constant as follows: holding time of 6 s, mold temperature of 110 °C taking as reference the heat distortion temperature (HDT) of 132 °C (ASTM D648 @ 1.82 MPa) [22], and cooling time of 25 s. According to published studies [23–28], the temperature of the metal insert, which can be controlled by insert pre-heating and mold temperature, is one of influencing factors on the joining strength of PMHs produced by injection overmolding. As the temperature of the metal insert increases, the thickness of the polymer frozen skin layer decreases, allowing for easier penetration of the polymer into the metal microcavities, providing a larger contact area between the polymer and metal and thus, higher joining strength. For this reason, the AA6061 substrates were pre-heated to 110 °C in an oven and manually positioned inside the mold cavity to shorten the heating of the metal substrate inside the mold before polymer injection. A waiting time of 60 s was applied before each molding cycle to ensure

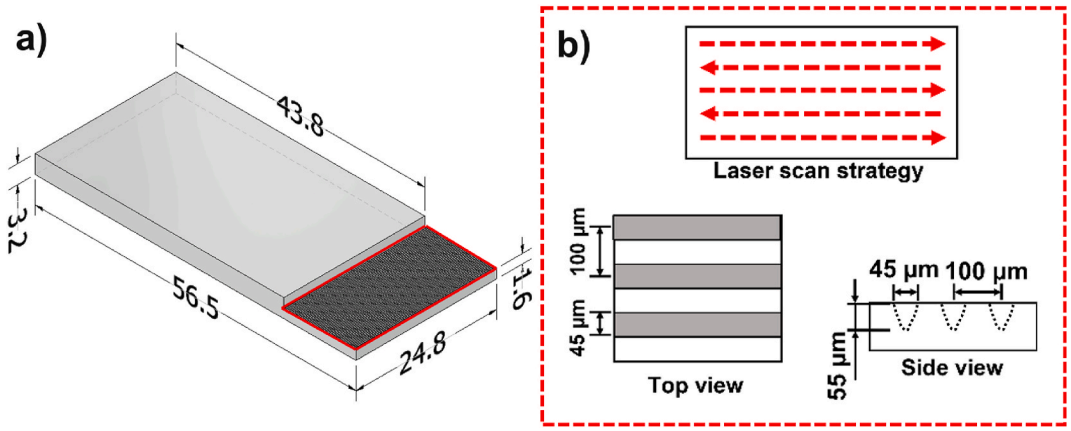

Fig. 1. Geometry and dimensions (in mm) of the AA6061 insert (a) and laser texturing micron-scale design (b).

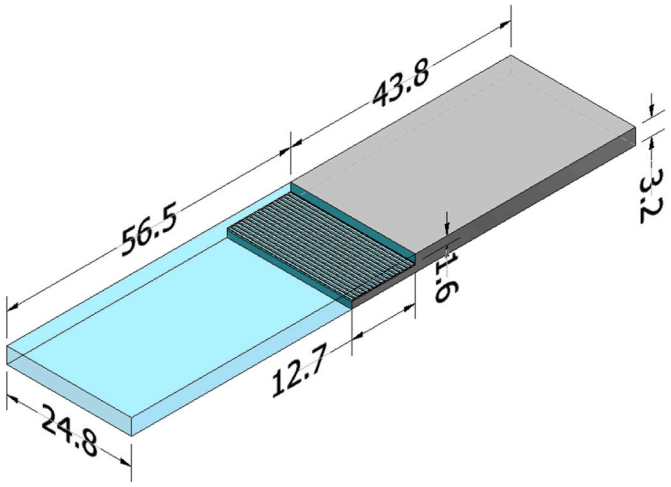

Fig. 2. Geometry and dimensions (in mm) of the injection overmolded PC/AA6061 hybrid joint specimen. AA6061 in light gray.

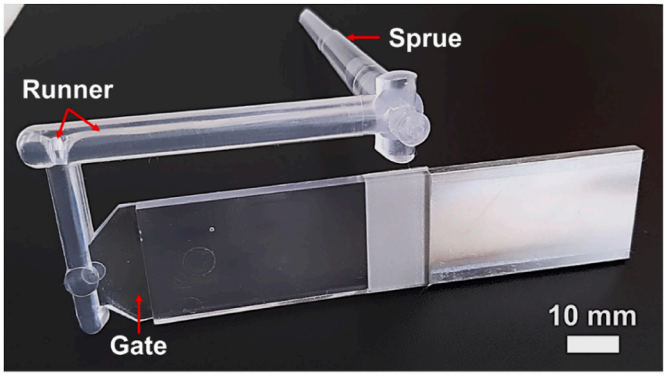

Fig. 3. Photograph of an injection overmolded PC/AA6061 joint specimen containing the sprue, runner and gate.

temperature equalization of the metal insert with the mold cavity. It is worth mentioning that pre-heating time can be optimized in future applications, for instance, by modifying the injection molding hardware. However, this has not been the focus of the current research.

The investigative response to the DoE was the joint ultimate lap-shear force (ULSF). The displacement at break was not evaluated as a response in this study, on the one hand, because of its direct proportionality with ULSF, and on the other hand, due to the fact that single lap shear specimens are known to induce secondary bending (i.e., out-of-plane stresses) [29,30] which would mask the evaluation of specimens damage tolerance. The study of fracture energy and fatigue damage tolerance of the current injection-overmolded specimens - which is out of the scope of this work - would require other testing specimen geometries, such as the single-leg bending specimen (SLB) [31,32]. SLB specimens are used to characterize interlaminar fracture of composites and adhesively bonded joints, accounting for a mixed-loading mode I/II adequate for metal-polymer hybrid joints [33]. ANOVA with a confidence level of 95 % was used to estimate the influence of each injection overmolding parameter and its interactions. Minitab 21 software (USA) was used for the statistical evaluation.

Table 1
Conditions of the 2^3 full factorial design of experiments used to produce PC/AA6061 hybrid joints via injection overmolding.

Condition	Barrel temperature [°C]	Injection speed [cm^3/s]	Holding pressure [bar]
C1	280	40	600
C2	330	40	600
C3	280	80	600
C4	330	80	1000
C5	280	40	1000
C6	330	40	1000
C7	280	80	1000
C8	330	80	600
Center Point	305	60	800

2.4. Lap-shear testing

The joining strength of the PC/AA6061 joints were evaluated by lap-shear testing, following an adaptation of the ASTM 1002 standard [34] using an Instron 5569 universal testing machine (Instron, USA) with a load cell of 50 kN and a distance between grips of 60 mm at a crosshead speed of 1.27 mm/min (0.05 inch/min). The specimens were conditioned at 23 °C ± 1 °C and 50 % ± 5 % relative humidity prior to tests, which were conducted at the same ambient conditions. Five replicate specimens were tested for each condition.

2.5. Confocal laser scanning microscopy

The surfaces of the machined and laser-textured AA6061 inserts and the polymer fracture surfaces of joints subjected to lap-shear testing were examined using a LEXT OLS 4100 confocal laser microscopy (Olympus, Japan) with a wavelength of 405 nm. The surface roughness, area and volume calculations were performed using the OLS4100 software.

The cross-section of the PC/AA6061 joints was examined through optical images captured with the confocal laser microscope to measure the penetration of the polymer into the grooves formed on the metal surface.

2.6. Scanning electron microscopy (SEM)

The polymer and metal fracture surfaces of joints subjected to lap-shear testing were examined using an FEI Inspect S50 scanning electron microscope (FEI, USA) equipped with secondary and backscattered electron detectors operated at an accelerating voltage of 15 kV, work distance of 10 mm and vacuum atmosphere. The analyzed samples were placed on carbon tapes and covered with gold before analysis.

2.7. Capillary rheometry

The melt shear viscosity of the PC at temperatures and rates similar to those applied in the injection overmolding of the joints was evaluated using a capillary rheometer SR50 (Instron, USA), with a capillary with a diameter of 1 mm and length to diameter (L/D) ratio of 30. The analyses were performed in the 10 s^{-1} to 10000 s^{-1} shear rate range at three different temperatures: 280 °C, 305 °C and 330 °C. The Rabinowitsch correction was employed to determine the shear rates at the inner wall of the capillary according to Equation (1) [35]:

$$\dot{\gamma}_w = \dot{\gamma}_A \left(\frac{3+b}{4}\right) \quad (1)$$

Where: $\dot{\gamma}_w$ is the shear rate at the wall, $\dot{\gamma}_A$ is the apparent shear rate at the wall, b = 1/n and n is the power law index.

2.8. Fatigue testing

The mechanical durability of the PC/AA6061 hybrid joint produced with optimized injection overmolding parameters (condition C4, Table 1) was estimated through dynamic fatigue testing using a MTS Bionix® universal testing machine (MTS, USA), operated under the following conditions: sinusoidal tensile mode (R = 0.1); frequency 5 Hz; and 4 load levels of 30 %, 40 %, 50 %, and 70 % ULSF [36,37]. The specimens were conditioned at 23 °C ± 1 °C and 50 % ± 5 % relative humidity prior to tests, which were conducted at the same ambient conditions. Three replicates were tested for each condition. The temperature measurement during the fatigue test was manually performed with a laser thermometer on the surface of the overlap area. No relevant variation in temperature was detected (25 °C ± 3 °C). The two-parameter Weibull distribution was selected to predict the fatigue life of the PC/AA6061 joints with two cycle levels (10^5 cycles and 10^6 cycles) and reliability of 90 %, 95 % and 99 %. These reliabilities values indicate that the probability of failure is between 1 % and 10 % [38]. The detailed steps for calculating the Weibull curves can be found in Refs. [39,40] for other different joining techniques and materials.

2.9. Hygrothermal aging

The hygrothermal stability of the PC/AA6061 hybrid joint produced with optimized injection overmolding parameters (condition C4, Table 1) was estimated based on the ASTM D1151. The joints were immersed in a deionized water bath at 80 °C for different periods; 1 day, 7 days, and 30 days, and then subjected to lap-shear testing. The weight of the joints was measured before and after aging to evaluate the water uptake. Five replicates specimens were tested for each condition.

2.10. Differential scanning calorimetry (DSC)

The glass transition temperatures (T_g) of the PC in unaged (control) and hydrothermal aged joints were measured by differential scanning calorimetry (DSC) using a Q2000 instrument (TA Instruments, USA). PC samples weighing 8.5 ± 0.2 mg extracted from the inner of the overlap region of joints were placed in aluminum crucibles and heated from 23 °C to 330 °C at 10 °C/min, under nitrogen atmosphere (50 mL/min). These analyses were performed in duplicate.

3. Results and discussion

3.1. Surface analysis of laser-textured AA6061 inserts

Fig. 4 shows images and height profiles obtained by laser scanning confocal microscopy of the machined and laser-textured surfaces of the overlap area of AA6061 inserts. The machined surface (Fig. 4a) showed surface crevices with an average depth of 0.8 ± 0.2 μm and roughness R_a and R_z values of 0.1 ± 0.01 μm and 0.4 ± 0.3 μm, respectively. The laser-textured surface (Fig. 4b) showed grooves with a depth of 55 ± 5 μm and roughness R_a and R_z values of 8 ± 0.5 μm and 27 ± 1 μm, respectively. Moreover, resolidified material can be observed on the laser-textured surface (Fig. 4b). During the laser scanning, the heated material is expelled from the radiated spot and displaced onto the surface and/or in the grooves next to it, thereby solidifying in place [41]. Resolidified material, commonly termed as recast material, can aid in the micro-anchoring of the polymer on the metal surface when properly attached to the metal surface [42]. The center-to-center distance between grooves remained constant at 100 μm as programmed, and the average groove width was 47 μm ± 2 μm, close to the diameter of the laser beam. Overall, the degree of uniformity of the grooves produced on the metal surface is within the expected range for the laser texturing technique [17–20].

The areas and the feature volumes of the analyzed surfaces (640 × 640 μm^2) were determined using the laser confocal microscope software and extrapolated to the nominal area of the insert recess (12.7 × 24.8 mm^2). Thus, the surface areas for the machined and laser-textured samples were 315 mm^2 and 715 mm^2, respectively. Analogously, the feature volumes for the surface of the machined and laser-textured samples were 0.22 mm^3 and 10.6 mm^3, respectively. Therefore, laser texturing produces a huge increase (approx. 4800 %) in the volume available for filling of the polymer into the metal surface grooves. However, it is worth mentioning that laser texturing and groove design parameters on the AA6061 inserts were chosen to induce failure by delamination (interfacial fracture) of PC/AA6061 joints on the lap shear testing in order to explore the effects of injection overmolding conditions on the joining strength.

3.2. Effects of injection overmolding conditions on the joining strength and interfacial structure of PC/AA6061 joints

Fig. 5 shows the mean values and respective standard deviations for the ultimate lap-shear forces (ULSF) of the PC/AA6061 joints produced by injection overmolding at different processing conditions (Table 1). ULSF values ranged from 191 ± 58 N to 2149 ± 127 N. All specimens failed by delamination, i.e., shear fracture at the metal-polymer interface. As mentioned before, this failure was intentionally induced. In other words, ductile failure of PC was avoided so that the effects of the injection overmolding conditions on the ULSF of joints could be evaluated.

According to the Pareto chart (Fig. 6) with a significance level (α) of 0.05, the factors barrel temperature, injection speed, and holding pressure exert significant influences on the ULSF of the PC/AA6061 joints, with the barrel temperature being the most significant factor, followed by the holding pressure, and the injection speed. Moreover, the Pareto chart showed that interactions between these factors are not statistically significant for the examined response.

Analysis of variance (ANOVA) with a 95 % confidence level was used to estimate the influence of the factors on the analyzed response. The ANOVA for the ULSF of PC/AA6061 joints is summarized in Table 2. The

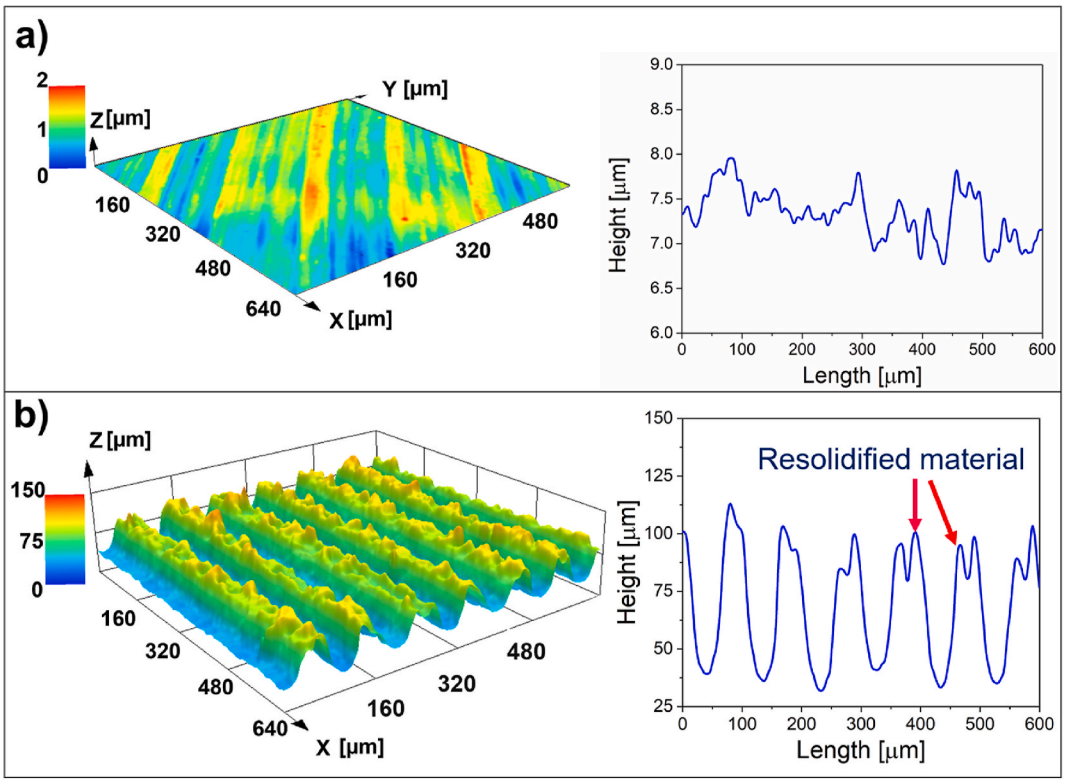

Fig. 4. Laser scanning confocal image and height profile of the machined (a) and laser textured (b) AA6061 surfaces.

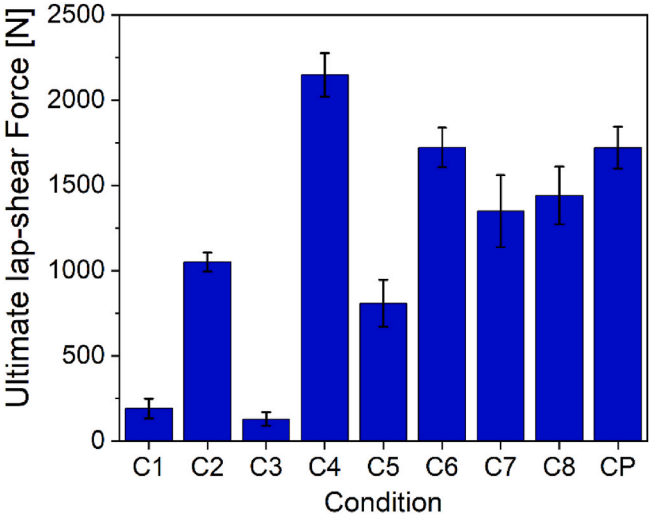

Fig. 5. Ultimate lap-shear force of PC/AA6061 joints for the selected injection overmolding conditions (see Table 1).

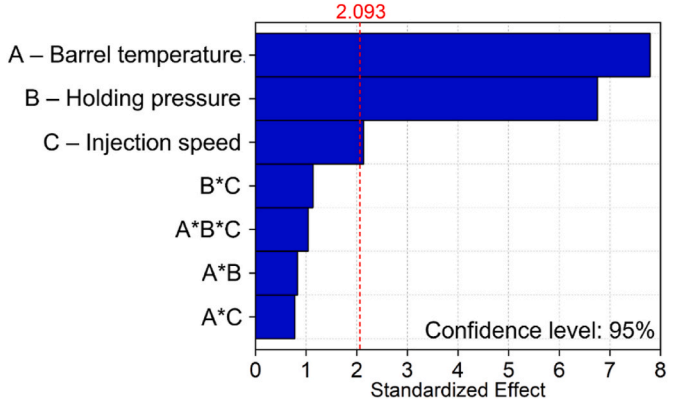

Fig. 6. Pareto chart of standardized effects for the ultimate lap-shear force of PC/AA6061 hybrid joints.

F-values for the main effects and their interactions are calculated by dividing the mean square of the effect of interest by the mean square of the error. The barrel temperature showed the highest effect on the statistical model with an F-ratio of 214.33, followed by the holding pressure with an F-value of 160.21 and injection speed with a minor significant value of 16.18. Furthermore, the p-value indicates if the parameter or interaction is significant to the model when α is lower than 0.05 (see Table 3).

The "mean of means" plot for ULSF in Fig. 7, which compares the arithmetic mean of the response ULSF for minimum (−1) and maximum (+1) levels of the factors with the total arithmetic mean of all samples, indicates that the three factors (barrel temperature, injection speed and holding pressure) have a positive effect on the ULSF of the PC/AA6061 joints. The statistical model produced an adjusted R^2 equal to 81 %. The regression model equation is given in Equation (2) [43], where the first term is the total variation in the response y, the second is the variation in the mean response, and the last is the residual value. Moreover, it should be noted in Fig. 7 that the center point is above the minimum (−1) and maximum (+1) factor levels. This suggests that relationships between the factors (barrel temperature, injection speed and holding pressure) and response (ULSF) are not linear in the 2^3 full factorial design of experiments used in this study. However, it is impossible to predict the curvature for predictor values that were not included in the design because there is no single surface that suits all model points. This may indicate that the use of a more complex statistical DoE with additional axial points able to model the curvature through a response surface design may be more suitable to accurately represent the dependence of the processing conditions. Furthermore, in injection molding, there is a

Table 2
Analysis of variance (ANOVA) of the ULSF for PC/AA6061 hybrid joints.

Source	DF	Adj SS	Adj MS	F-Value	p-Value
Model	8	10952755	1369094	56.61	0.001
Linear					
Barrel temperature	1	5183600	5183600	214.33	0.001
Injection speed	1	391408	391408	16.18	0.001
Holding pressure	1	3874731	3874731	160.21	0.001
2-Way Interactions					
Barrel temperature*Injection speed	1	52311	52311	2.16	0.159
Barrel temperature*Holding pressure	1	60697	60697	2.51	0.131
Injection speed*Holding pressure	1	112039	112039	4.63	0.055
3-Way Interactions					
Barrel temperature*Injection speed*Holding pressure	1	94368	94368	3.90	0.064
Error	18	435327	24185		
Total	26	11388082			

Table 3
Fatigue life of PC/AA6061 joints predicted at two cycle levels by the two-parameter Weibull model with reliability of 90 %, 95 % and 99 %.

Model	At 10^5 cycles		At 10^6 cycles	
	Force [N]	ULSF [%]	Force [N]	ULSF [%]
Weibull (R: 90 %)	1271	59	740	34
Weibull (R: 95 %)	1250	58	746	35
Weibull (R: 99 %)	1208	56	756	35

complex interdependence of temperature, flow rate and pressure on the viscosity and shrinkage parameters that govern the filling of the polymer in the cavities of the metal surface and resulting residual stresses in the polymer component [10,44]. Therefore, the explanation of the deviation of the center point from the linearity is a complex matter; a detailed statistical evaluation of the correlation of the injection overmolding conditions on the joining strength of hybrid joints is out of the scope of this manuscript. This topic will be addressed in future work.

The response ULSF was maximized for "higher is better" using Minitab 21 and thus the condition C4 (Table 1) was selected as the optimized condition for further experiments, with the following parameters: barrel temperature 330 °C, injection speed 80 cm^3/s and holding pressure 1000 bar.

$$\sum (y_i - \bar{y})^2 = \sum (\hat{y}_i - \bar{y})^2 + \sum (y_i - \hat{y}_i)^2 \quad (2)$$

The degree of filling of the PC into the grooves of the AA6061 surface was dependent on the injection overmolding conditions. Increasing the factors that exert a positive influence on the ULSF, i.e., barrel temperature, injection speed, and holding pressure, resulted in greater filling of the PC into the grooves of the AA6061 surface, as shown in Fig. 8a–c, respectively, for the polymer fracture surfaces and cross-sections of PC/AA6061 joints injection overmolded in the conditions C1, CP and C4 (see Table 1). The joint that presented the lowest ULSF value (condition C1) exhibited the lowest filling depth of the polymer into the metal grooves of 25 μm ± 1 μm, which corresponds to approximately 50 % of the average groove depth (55 μm ± 5 μm). Condition CP resulted in a polymer filling depth of 41 μm ± 3 μm, corresponding to approximately 75 % of the average groove depth. Condition C4, with the highest ULSF value, resulted in filling depth of 55 μm ± 5 μm corresponding to complete filling of the PC into the grooves on the metal surface.

The ultimate lap-shear force (ULSF) of the PC/AA6061 joints presented a linear increase with the filling depth of the PC into the grooves of the AA6061 surface (Fig. 9). Increasing the filling depth of the PC into the grooves of the AA6061 increases the interference volume between the polymer and metal components, resulting in PC/AA6061 joints that are mechanically stronger.

Effects of injection overmolding conditions on the joining strength of injection overmolded PMH joints have been explored in the literature for other combinations of materials and with various types of metal surface preparation. In general, proportionality has been between the mechanical strength of the joints and the polymer filling degree into the metal surface microcavities [13,25–27,45]. Zhao et al. [13] studied overlap joints of 30 wt% glass fiber reinforced poly(butylene terephthalate) (PBT-30GF) and laser-textured AA5052 and found that the filling degree and joining strength increased with packing and holding pressures, whereas the barrel temperature only positively affected the joining strength for low packing pressure. Lucchetta et al. [45] observed a positive effect of injection speed on the filling degree and mechanical

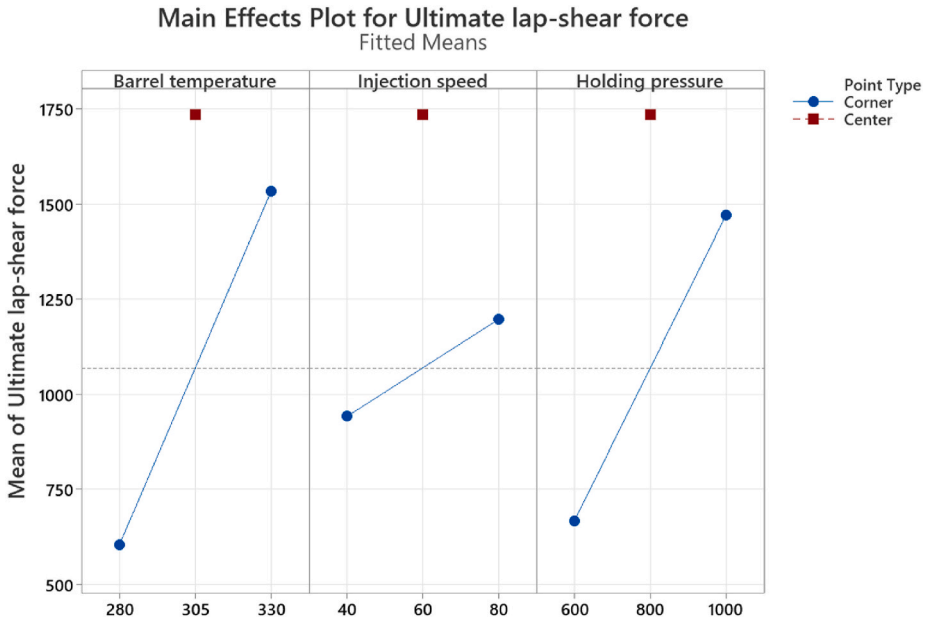

Fig. 7. Main effect plots illustrating the influence of the injection overmolding parameters (barrel temperature, injection speed, and holding pressure) on the ULSF of PC/AA6061 joints.

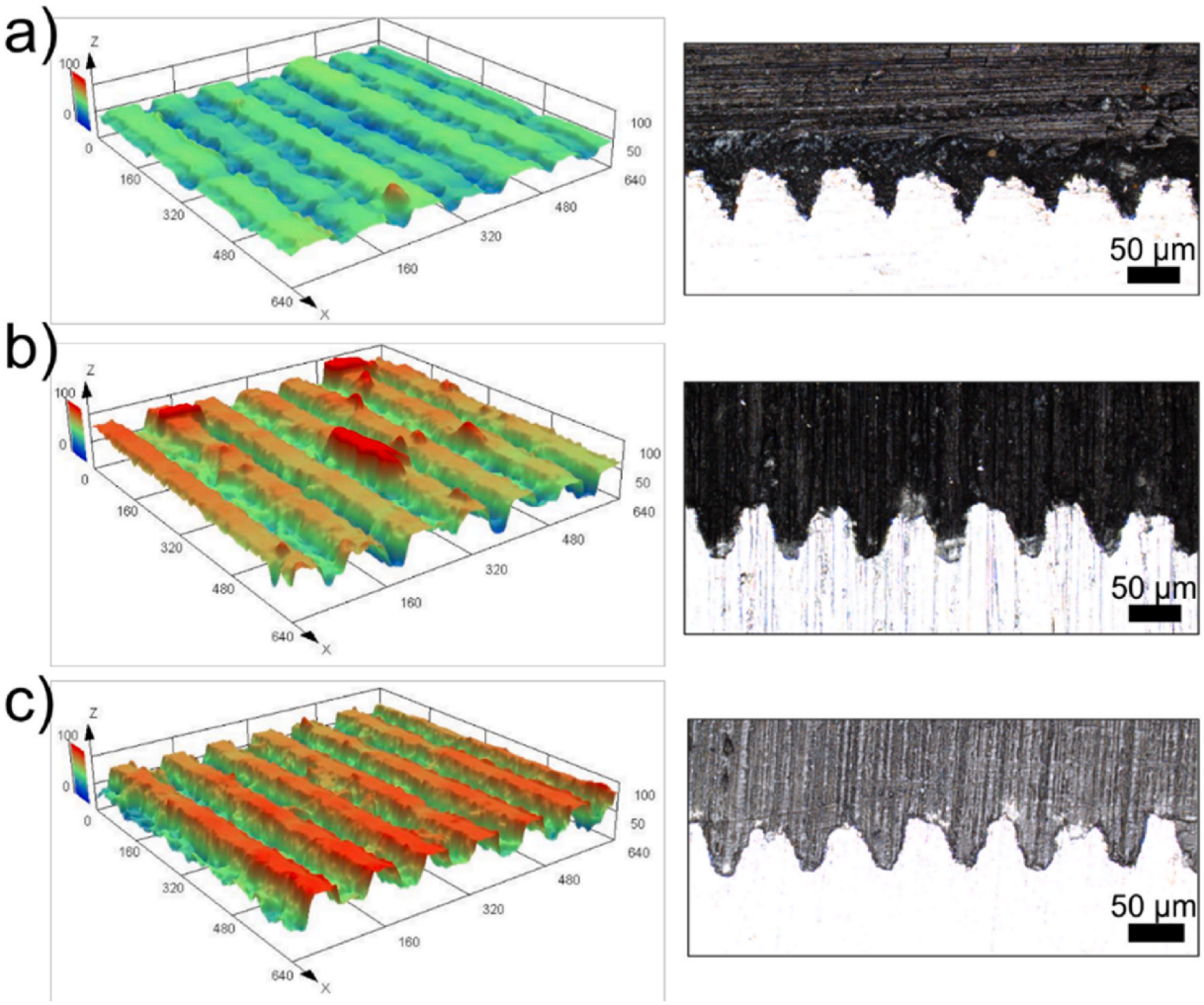

Fig. 8. On the left-hand side laser confocal microscopy images of polymer fracture surfaces and the right-hand side images obtained in the laser confocal microscope of the cross-section of PC/AA6061 joints injection overmolded under the following conditions: a) C1 (minimum levels); b) (center point - CP); and c) C4 (maximum levels). In the cross-section images, metal and polymer parts appear as light and dark, respectively.

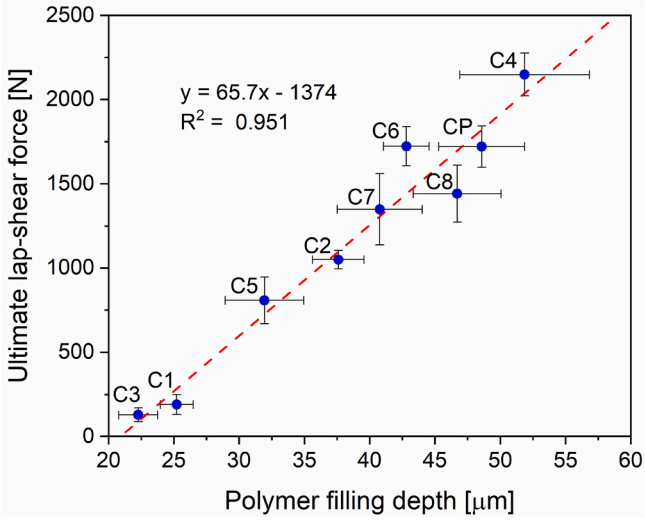

Fig. 9. Ultimate lap-shear force of PC/AA6061 joints injection overmolded under different conditions as a function of the filling depth of the PC into the AA6061 grooves.

strength of joints of 40 wt% glass fiber reinforced poly(phenylene sulfide) (PPS-40GF) with sand-blasted AA6082 inserts.

The degree of filling of the PC into AA6061 surface grooves depends ultimately on the rheology of the molten polymer. It should be noted no rheological approaches are currently available in the scientific literature for predicting polymer filling in microcavities on the metal surface in polymer-metal joints. Nevertheless, capillary rheometry can provide valuable qualitative data on the viscosity of the molten polymer under conditions similar to those experienced in the injection overmolding of PC/AA6061 joints. The shear viscosity curves for the PC at 280 °C, 300 °C and 330 °C are shown in Fig. 10. The range of shear rate to which the polymer was exposed in the polymer-metal joining zone during injection overmolding is depicted as a light gray area. For this estimation, Equation (3) was used, assuming that the PC melt flow in the overlap area (W = 24.8 mm and H = 1.6 mm) is similar to a pressure-driven isothermal flow of a power law fluid in between parallel plates, where Q is the flow rate (injection speed), W is the width and H is the thickness of the channel [46]. The grooves structures on the metal surface were not considered for simplification purposes.

$$\dot{\gamma}_w = \left(\frac{2n+1}{n}\right)\frac{2Q}{W.H^2} \tag{3}$$

As expected, the melt shear viscosity of PC decreases with temperature and shear rate applied. The increase in the temperature increases

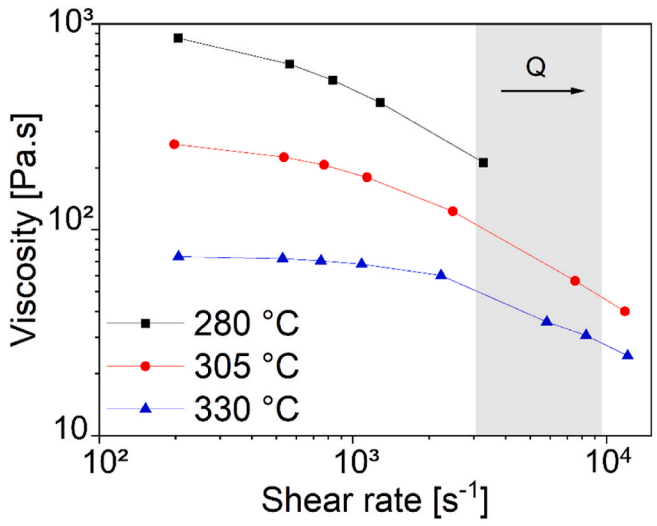

Fig. 10. Capillary rheometer viscosity curves of PC (LEXAN 103) at temperatures similar to that employed in the injection overmolding of the joints (see Table 1). Viscosity data at 280 °C were measured at shear rates below 2 x 10^3 s^{-1} since the upper limit of the rheometer load cell was reached. The range of shear rate to which the polymer is exposed in the polymer-metal joining zone during injection overmolding is depicted as a light gray area.

the mobility of polymer chains and the higher free volume between polymer chains generates less friction, decreasing viscosity. The viscosity lowers as shear rates increase because, at high shear rates, the polymer chains tend to align in the flow direction, reducing the degree of entanglement and flow resistance [46,47]. By examining the viscosity curves and the shear rate estimated for the joining region, melt viscosities ranging from 215 Pa s to 50 Pa s are obtained, depending on the injection molding conditions. Moreover, when the molten polymer hits the surface of the metal insert at lower temperature (such as the injection molding conditions used in this study), a thin frozen skin layer is formed; the magnitude of the thickness, depending on the injection overmolding conditions, will restrict the further penetration of the polymer into the grooves of the metal. Thus, increasing barrel temperature decreases the viscosity of the polymer during the cavity filling, reducing the thickness of the frozen layer and facilitating the penetration of the polymer into the metal grooves. Increasing injection speed results in a higher shear rate at the polymer-metal interface and a shorter filling time, which reduces the viscosity of the polymer melt and the thickness of the frozen layer, improving the penetration of polymer into metal grooves. Increased holding pressure leads to increased deformation of the frozen layer during the packing process, allowing for higher polymer penetration into the metal grooves. Therefore, the maximum values of these parameters (barrel temperature, injection speed and holding pressure) assist in filling the polymer into the grooves on the metal surface, as shown in Fig. 8c for condition C4 (Table 1). Furthermore, holding pressure compensates for the polymer thermal contraction during the solidification in the mold cavity, helping to keep the polymer filled into the metal grooves. Still, PC is an amorphous polymer, so its volumetric shrinkage during injection molding is considerably low, allowing the metal grooves to remain completely filled with PC after joint cooling.

The lap shear strength (ULSS) of the PC/AA6061 joint injection overmolded in the optimized condition (C4), which resulted in complete filling of the PC in the grooves of the AA6061 (Fig. 8c) was estimated to be equal to 7.2 ± 0.5 MPa, based on the ULSF of 2149 ± 127 N (Fig. 9) and the nominal overlap area of 12.7 × 24.8 mm^2. It should be noted that the side wall of the AA6061 cannot be considered as part of the contact area. Preliminary injection overmolding studies on joints prepared with non-textured AA6061 parts have indicated a lack of adhesion in the overlap area. This magnitude of joining strength is comparable to other PMH joints produced by injection overmolding with metal inserts structured by laser-texturing [13–15,17–20], as well as those with metal inserts structured by sand-blasting [23–25,45,48–51], anodizing [52–55], additive manufacturing [56], electron beam surface structuring [16], chemical treatments [51,57–61] and silanization [62–65].

3.3. Fracture analysis of PC/AA6061 joints

Fig. 11 shows photographs of the fracture surfaces after lap-shear testing on PC/AA6061 joints produced under C1, CP and C4 injection overmolding conditions. As mentioned before, all joints failed macroscopically by delamination. However, at microscopic level, the fracture mechanism depended on the injection molding conditions and therefore on the degree of filling of the polymer into the grooves on the metal surface. The joint produced with condition C1 failed locally with adhesive fracture (Fig. 11a); the lower penetration of polymer into the metal laser-formed grooves led to lower level of micro-anchoring of the polymer on the metal surface and thus lower ULSF. The joint produced with the center point condition (CP) with intermediate polymer filling level exhibits signs of cohesive metal fracture, which remained bonded to the polymer side (Fig. 11b, red squares). Under the optimized injection overmolding condition (C4) with complete filling of polymer into the metal grooves, the cohesive fracture of the metal covered a larger area (shown by the red squares, Fig. 11c).

Fig. 12a–c shows SEM images of the fracture surface on the metal part of the PC/AA6061 joint produced with the optimized injection overmolding condition (C4). There are signs of metal cohesive fracture. It is possible to observe that a portion of the metal strips in between the grooves formed by laser texturing has been displaced in the load direction (Fig. 12b) and that another portion of the strips has been pulled from the metal (Fig. 12c).

Fig. 13a–c shows the fractured surface on the polymer side of the PC/AA6061 joint produced with the optimized injection overmolding condition (C4) viewed by SEM images with backscattered electrons (BSE) and energy-dispersive X-ray spectroscopy (EDX) mapping. Pieces of strips detached from the metal surface adhered on the polymer side can be seen in the zone of cohesive fracture (Fig. 13a and b). At higher magnification (Fig. 13c and d), one can also observe metal fragments adhered on the polymer side, which can be attributed to the recast material formed during laser texturing (Section 3.1, Fig. 4b).

Therefore, it seems that the main adhesion mechanism of the PC/AA6061 injection-overmolded joints is the mechanical interlocking of the polymer into the metal grooves. This s has been reported in the literature for injection overmolded PMH joints with different material combinations. Rodríguez-Vidal et al. [42] observed a dependency between the density and aspect ratio (depth/diameter) of laser-formed grooves as well as the recast material height on lap-shear strength of joints with laser-textured low-alloy steel HC420 substrate and glass fiber reinforced polyamide 6. Byskov-Nielsen [17] observed increased lap-shear strength with a higher density of dimples formed on the metal surface by laser texturing for joints of stainless steel (DIN 1.4301) and a composite of polyphenylene sulfide (PPS) reinforced with 40 wt% glass fiber. Xu et al. [14] observed that a higher density of grid-shaped laser-structured grooves increases the lap-shear strength of AA5052 and PBT-30GF joints. Furthermore, one can speculate that the carbonyl groups on the PC chains form Al–*O*–C chemical (covalent) bonds with the alumina layer on the surface of AA6061, as suggested by the studies of Li et al. [66] and Goushegir et al. [67]. However, the analysis of the chemical bond formation as an adhesion mechanism is out of the scope of this work and will be addressed in future publications.

3.4. Fatigue behavior of PC/AA6061 joints

The force-life (F–N) curves are shown in Fig. 14 along with two-parameter Weibull model fitting. Joints subjected to 70 %, 50 %, and 40 % ULSF failed after 70 ± 7 (x10^3), 256 ± 17 (x10^3), 464 ± 11 (x10^3)

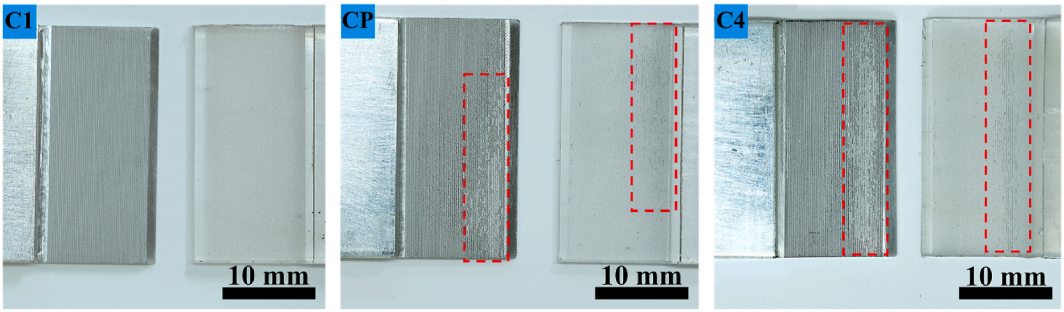

Fig. 11. Fracture surface photographs of PC/AA6061 joints produced under injection overmolding conditions C1, CP and C4 (see Table 1). Red squares indicate a fracture of the strips formed on the metal surface.

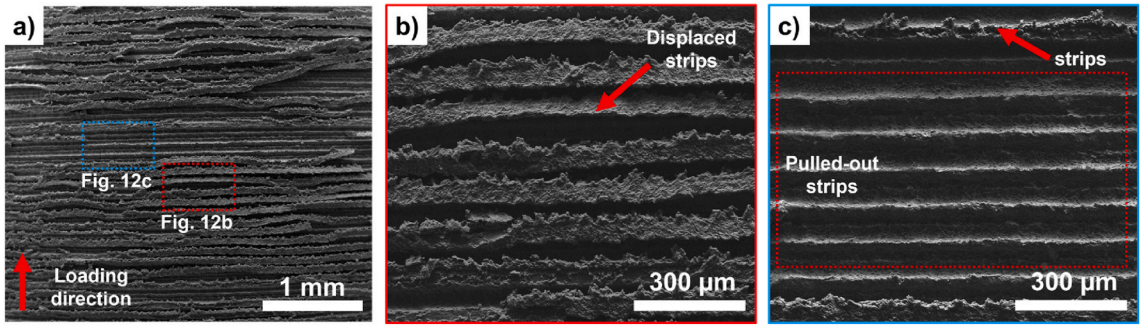

Fig. 12. Scanning electron microscopy (SEM) images (secondary electrons) of the metal fracture surface of the PC/AA6061 joint produced with optimized injection overmolding condition (C4). a) Image with indications of cohesive fracture; b) Magnification of the region marked with red square where the strips were displaced; c) Magnification of the region marked with blue square where the strips were pulled out.

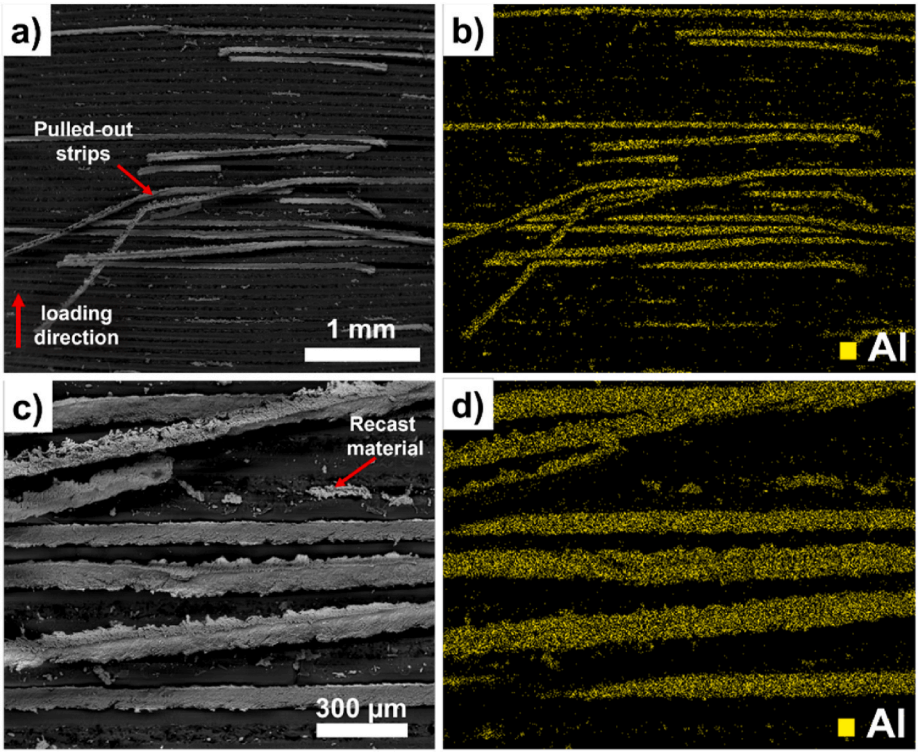

Fig. 13. Scanning electron microscopy (SEM) images with backscatter electrons (BSE) (left side) and energy-dispersive X-ray spectroscopy (EDS) mapping of aluminum (right side) of the fracture surface on the polymer side of a PC/AA6061 joint produced with optimized injection overmolding condition (C4). Low (a and b) and high (c and d) magnifications.

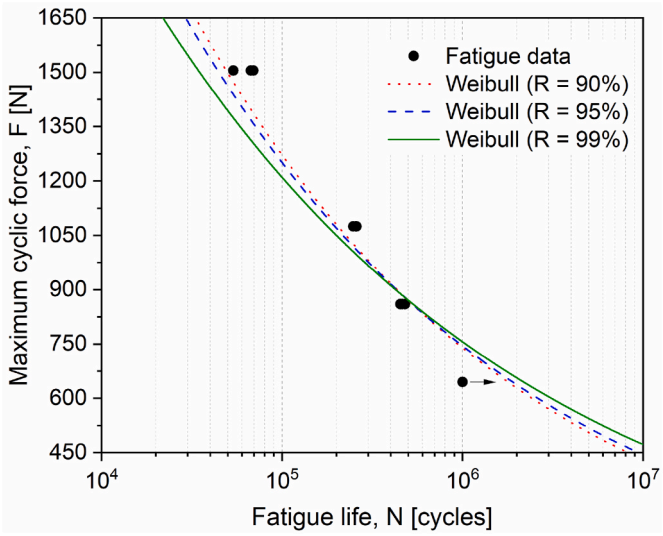

Fig. 14. Force-life (F–N) curve in tensile mode (R = 0.1) at 5 Hz at load levels of 30 %, 40 %, 50 %, and 70 % ULSF for PC/AA6061 joints produced in the optimized injection overmolding condition (C4). The experimental data were fitted by two-parameter Weibull models with reliability of 90 %, 95 % and 99 %.

cycles, respectively, by net-tension fracture of the PC part near the end of the AA6061 insert (Fig. 15), whereas joints subjected to 30 % ULSF endured 10^6 cycles without failure (the so-called run-out specimens and represented by the arrows in Fig. 14), but with a visual onset of a transverse crack nucleating in the PC part near the end of the AA6061 insert. On the other hand, for all loading levels applied, the polymer-metal interface of the joints remained intact, which attests to outstanding interfacial mechanical durability under cyclic loading.

The region where PC underwent fracture during fatigue testing is subjected to a combined tensile (principal) and bending (secondary) stress, typical of single-lap joints [68–70]. If one makes an approximation that this region, with a cross-sectional area of 24.8 × 1.6 mm^2 (width x thickness), is subjected to uniaxial tensile stress, then stresses of approximately 38 MPa, 27 MPa, 22 MPa, and 16 MPa would be developed, respectively, for 70 %, 50 %, 40 %, and 30 % ULSF loading. Although the fatigue behavior of PC is enhanced by the high degree of chain orientation resulting from injection overmolding [71], under these fatigue-loading conditions PC is found to undergo brittle fracture [72,73], and this has been attributed to the plastic deformation mechanisms of PC - shear bands and crazing – which do not develop sufficiently under these cyclic loading levels; they rather act as stress

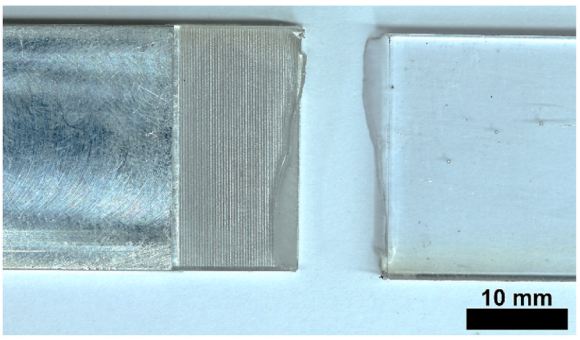

Fig. 15. Photograph exemplifying the failure mode of the PC/AA6061 joints injection overmolded in the optimized condition (C4) subjected to fatigue (tensile; R = 0.1; 5 Hz) testing at loading levels of 40 %, 50 % and 70 % of the ULSF. Detail of the transverse brittle fracture of PC near the end of the metal insert.

concentrators through which a crack nucleates and propagates in a brittle manner [74]. Fig. 16 shows details of the brittle fracture of the PC part. Two distinctive regions can be observed in the global image of the fracture surface in Fig. 16a. A characteristic crack initiation surface (Fig. 16b) and a crack propagation surface delineated by fatigue beachmarks (Fig. 16c) can be observed on the region marked with a red rectangle. On the region marked with a yellow rectangle, there are signs of the formation of crazes along with crack propagation (Fig. 16d and e).

Based on the Weibull analysis, the fatigue lives of the PC/AA6061 joints for 10^5 and 10^6 cycles with reliability of 99 % were, respectively, 1208 N (56 % of the ULSF) and 756 N (35 % ULSF). For the sake of comparison, these fatigue lives are over the aviation requirements for structural safety which demands a minimum fatigue life of 30 % of the ULSF [75].

It should be noted that the joints subjected to a cyclic loading of 640 N (30 % of ULSF), below the predicted using Weibull analysis with reliability of 99 % at 10^6 cycles, that is, 756 N (35 % of ULSF), did not fracture in the fatigue test. These run-out joints were subsequently subjected to quasi-static lap-shear testing resulting in a 61 % residual strength. These results indicate that fatigue damage was introduced and accumulated during cyclic loading at the selected level of 30 % of the ULSF.

Fatigue strength studies on polymer-metal joints produced by injection overmolding are scarce in the literature. Nevertheless, the fatigue behavior of the PC/AA6061 joints is comparable or superior to those reported in the literature for similar systems. For instance, Zhao et al. [61] evaluated the fatigue strength of injection overmolded joints of PBT-30GF with AA5052 nanostructured by chemical and hot water treatment. They observed that optimized joints reached 10^5 cycles when subjected to milder conditions than those employed in this study, with cycling at 2 Hz and a cyclic tensile load of 15 % of the ULSF.

3.5. Hygrothermal aging of PC/AA6061 joints

The PC/AA6061 results after hygrothermal aging are shown in Fig. 17. The ULSF showed a 10 % decrease after 1 day, which were recovered for longer times of hygrothermal aging. After 7 days of hygrothermal aging, the PC/AA6061 joint attained saturation (0.19 %) for water uptake. Like unaged joints, hygrothermal aged joints exhibited delamination with mixed failure (adhesive-cohesive) after the lap-shear testing.

The hygrothermal aging conditions employed in this study are expected to influence more significantly the PC component, i.e., water absorption is negligible. Accordingly, PC samples extracted from unaged and aged joints were further investigated. The glass transition temperatures (T_g) of these samples are shown in Fig. 18. The T_g of all PC samples, defined by an endothermic inflection of the heat flow curve at about 150 °C, are not significantly affected by the hygrothermal aging. However, the unaged PC sample exhibits an endothermic event immediately above T_g (black arrow, Fig. 18), which does not appear for the aged samples. The observed endothermic phenomenon is a distinctive feature associated with the relaxation of polymer chains. These chains, initially in a glassy state, exhibit increased mobility upon heating above T_g. The endothermic response is attributed to the loss of polymer chain orientation induced by the injection molding process, which subjects the material to high shear and rapid cooling rates [76–78]. Therefore, in addition to water absorption the hygrothermal aging of the PC/AA6061 joints resulted in the relaxation of the PC chains, which can lead to physical aging. Indeed, these two phenomena are observed when an amorphous, glassy polymer such as PC is exposed to extended hygrothermal aging, particularly around its glass transition temperature [79]. While water diffusion causes the polymer to expand and consequently reduce its stiffness, physical aging does the opposite, causing the polymer to reduce this volume (densification) and increase its stiffness. The net effect will depend on the balance of these two opposite phenomena.

Thus, a possible explanation for the decrease in the residual ULSF of

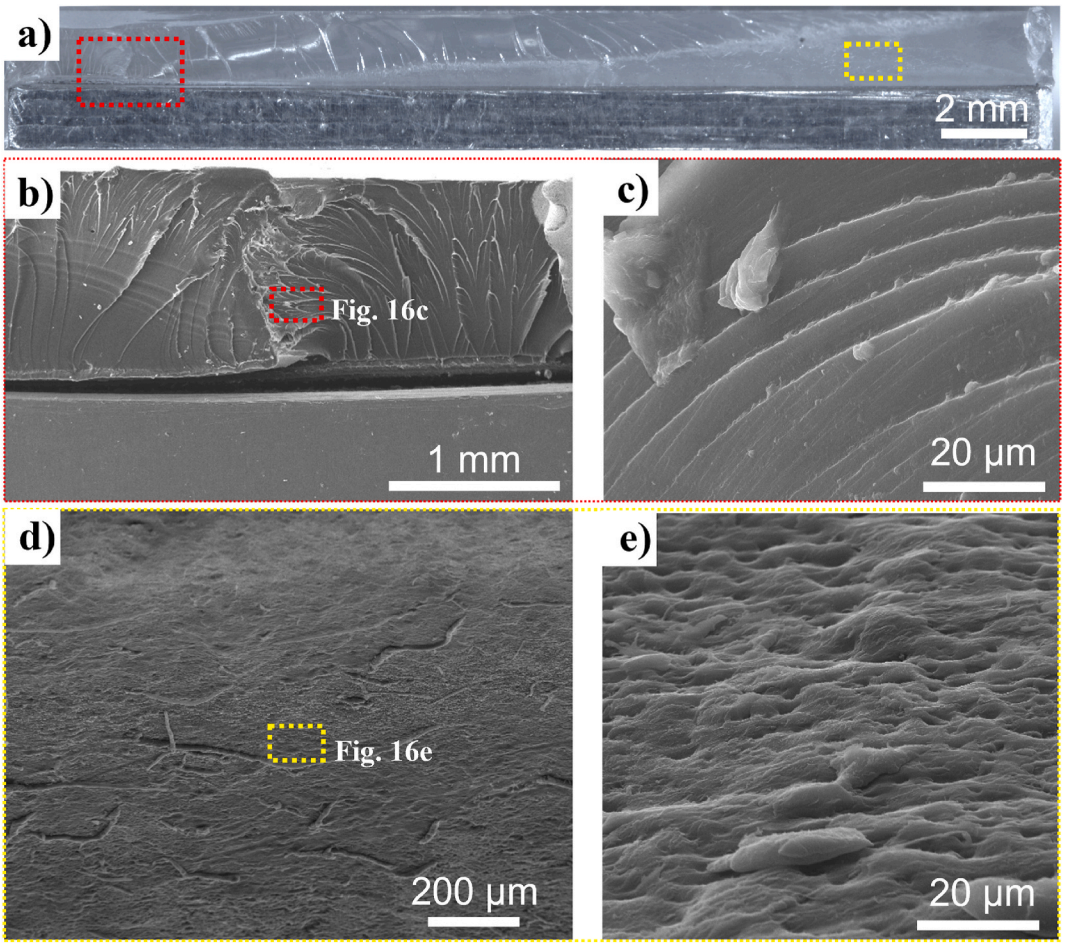

Fig. 16. Details of the brittle fracture of the PC part. a) Photograph overview of the PC/AA6061 cross-section fracture surfaces; b-e) SEM images of the crack initiation spot (b), beachmarks (c) and crazing marks (d–e) of the crack propagation path.

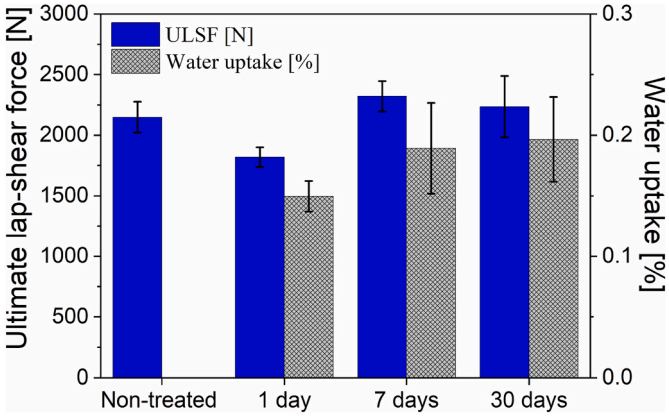

Fig. 17. Ultimate lap-shear force (ULSF) and water uptake of PC/AA6061 joints injection overmolding with optimized condition (C4) subjected to accelerated hygrothermal aging through immersion in water bath at 80 °C for different periods.

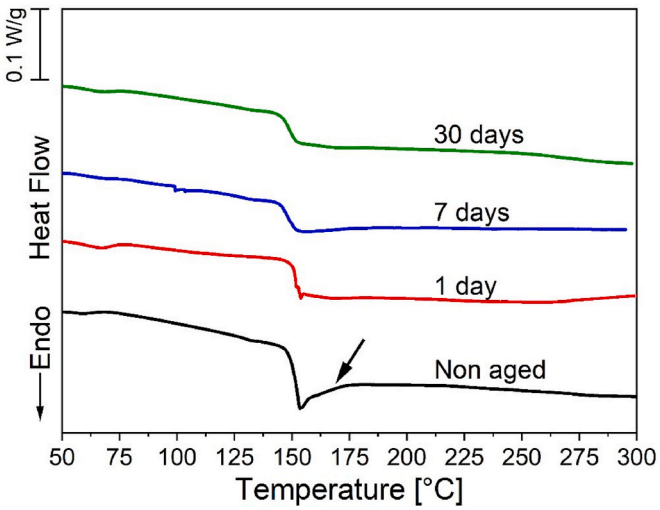

Fig. 18. DSC curves (heating at 10 °C/min) showing the T_g of PC samples extracted from PC/AA6061 joints subjected to hygrothermal aging by immersion in water at 80 °C for 1, 7 and 30 days. The data for unaged PC sample (control) is included for comparison.

PC/AA6061 joints after 1 day and recovery after 7 days of hygrothermal aging (Fig. 18) may be related to the balance on the PC stiffness caused by water absorption and physical aging. This trend of decrease followed by recovery in the joining strength with the aging time has been observed in other studies. The study conducted by Borba et al. [80] investigated the behavior of friction riveted joints between Ti6Al4V and CF-PEEK materials. The joints were subjected to an aging process at a temperature of 71 °C and a relative humidity of 95 % for durations of 3, 14, and 28 days. The researchers noted a decrease in residual ULSF after 3 and 14 days, followed by an increase after 28 days. The decrease in

residual strength was related to the phenomenon of water absorption, which resulted in the plasticization of the polymer chains. Furthermore, according to the authors, there is a correlation between the increase in residual strength after a period of 28 days and the corresponding increase in the degree of crystallinity or molecular rearrangement due to aging.

4. Conclusions

An in-depth study was carried out on the correlation between processing conditions, adhesion mechanisms, as well as short and long-term mechanical performances, and hygrothermal stability of injection overmolding hybrid overlap joints of polycarbonate (PC) and laser-textured aluminum alloy AA6061.

Using design of experiments (DoE) and analysis of variance (ANOVA), it was shown that the injection overmolding parameters barrel temperature, holding pressure and injection speed played positive effects on the filling depth of polymer into the laser-textured grooves on the metal surface, which directly contributed to increase the ultimate lap-shear force (ULSF) of the joints. Under optimized injection overmolding conditions – barrel temperature 330 °C, holding pressure 1000 bar, injection speed 80 cm^3/s (with mold temperature fixed at 110 °C) – joints reached ULSF of 2149 N ± 53 N resulting in a lap-shear strength of 7.2 ± 0.5 MPa (overlap area of 12.7 mm × 24.8 mm), which is comparable to other related joints shown in the literature. PC/AA6061 joints exhibited mixed (adhesive and cohesive) failure with pull-out of the metal adhered to the polymer side in the lap-shear test.

PC/AA6061 injection overmolded hybrid joints showed excellent mechanical durability in fatigue tests withstanding 10^6 cycles at 30 % ULSF. Based on the two-parameters Weibull analysis, the fatigue lives of the joints were estimated to be 56 % ULSF and 35 % ULSF for 10^5 and 10^6 cycles, respectively, with 99 % of reliability. These are outstanding results because they conform to the severe test standards of industries, such as in aircraft.

Moreover, injection overmolded hybrid joints also exhibited excellent hygrothermal stability after aging at 80 °C for 30 days, with no significant change in the ULSF. DSC studies on hygrothermal aged PC samples suggested two competing mechanisms during hygrothermal aging of joints - water absorption and physical aging of the polymer - which appear to balance the stiffness of the PC, with negligible effect on the joining strength of aged specimens. This is essential for ensuring component durability and efficacy under high temperature and humidity conditions for industries such as aerospace.

Declaration of competing interest

The authors declare that they have no known competing financial interests or personal relationships that could have appeared to influence the work reported in this paper.

Data availability

Data will be made available on request.

Acknowledgments

This study was supported by FAPESP - São Paulo Research Foundation, Brazil (grants # 2018/24296-0 and 2017/17188-3), CAPES - Coordenação de Aperfeiçoamento de Pessoal de Nível Superior - Brazil (grant # 88887.569948/2020-00, and global budget code 001) and CNPq - National Council for Scientific and Technological Development, Brazil (grants # 309258/2020-0 and 164791/2018-3). This study was financed in part by the Coordenação de Aperfeiçoamento de Pessoal de Nível Superior - Brasil (CAPES) - Finance Code 001. The authors gratefully acknowledge financial support from the Austrian aviation program "TAKEOFF" (PILOT, grant number 852796, 2018) and the BMK - The Austrian Ministry for Climate Action, Environment, Energy, Mobility, Innovation and Technology. The authors are grateful to the Laboratory of Structural Characterization (LCE/DEMa/UFSCar) for use of the general facilities.

References

[1] Lyu MY, Choi TG. Research trends in polymer materials for use in lightweight vehicles. Int J Precis Eng Manuf 2015;16:213–20. https://doi.org/10.1007/s12541-015-0029-x.
[2] Lambiase F, Scipioni SI, Lee CJ, Ko DC, Liu F. A state-of-the-art review on advanced joining processes for metal-composite and metal-polymer hybrid structures. Materials 2021;14. https://doi.org/10.3390/ma14081890.
[3] Grujicic M, Sellappan V, Omar MA, Seyr N, Obieglo A, Erdmann M, Holzleitner J. An overview of the polymer-to-metal direct-adhesion hybrid technologies for load-bearing automotive components. J Mater Process Technol 2008;197:363–73. https://doi.org/10.1016/j.jmatprotec.2007.06.058.
[4] Belei C, Pommer R, Amancio-Filho ST. Optimization of additive manufacturing for the production of short carbon fiber-reinforced polyamide/Ti-6Al-4V hybrid parts. Mater Des 2022;219. https://doi.org/10.1016/j.matdes.2022.110776.
[5] Green ML, Espinal L, Traversa E, Amis EJ. Materials for sustainable development. MRS Bull 2012;37:303–8. https://doi.org/10.1557/mrs.2012.51.
[6] Oliveira GHM, Belei C, de Carvalho WS, Canto LB, Amancio-Filho ST. On the fully additive manufacturing of PC/AlSi10Mg hybrid structures. Mater Lett 2023;330:133378. https://doi.org/10.1016/j.matlet.2022.133378.
[7] Gohil M, Joshi G. Perspective of polycarbonate composites and blends properties, applications, and future development: a review. In: Green Sustainable process for chemical and Environmental engineering and science. Elsevier; 2022. p. 393–424. https://doi.org/10.1016/B978-0-323-99643-3.00012-7.
[8] Miller WS, Zhuang L, Bottema J, Wittebrood AJ, De Smet P, Haszler A, Vieregge A. Recent development in aluminium alloys for the automotive industry. Materials Science and Engineering: A 2000;280:37–49. https://doi.org/10.1016/S0921-5093(99)00653-X.
[9] Grujicic M, Sellappan V, Arakere G, Seyr N, Obieglo A, Erdmann M, Holzleitner J. The potential of a clinch-lock polymer metal hybrid technology for use in load-bearing automotive components. J Mater Eng Perform 2009;18:893–902. https://doi.org/10.1007/s11665-008-9325-2.
[10] Vasconcelos RL, Oliveira GHM, Amancio-Filho ST, Canto LB. Injection overmolding of polymer-metal hybrid structures: a review. Polym Eng Sci 2023. https://doi.org/10.1002/pen.26244.
[11] Grujicic M, Sellappan V, Arakere G, Seyr N, Erdmann M. Computational feasibility analysis of direct-adhesion polymer-to-metal hybrid technology for load-bearing body-in-white structural components. J Mater Process Technol 2008;195:282–98. https://doi.org/10.1016/j.jmatprotec.2007.05.016.
[12] Lucchetta G, Marinello F, Bariani PF. Aluminum sheet surface roughness correlation with adhesion in polymer metal hybrid overmolding. CIRP Ann Manuf Technol 2011;60:559–62. https://doi.org/10.1016/j.cirp.2011.03.073.
[13] Zhao S, Kimura F, Kadoya S, Kajihara Y. Experimental analysis on mechanical interlocking of metal–polymer direct joining. Precis Eng 2020;61:120–5. https://doi.org/10.1016/j.precisioneng.2019.10.009.
[14] Xu R, Xie Y, Li R, Zhang J, Zhou T. Direct bonding of polymer and metal with an Ultrahigh strength: laser treatment and mechanical interlocking. Adv Eng Mater 2021;23:1–11. https://doi.org/10.1002/adem.202001288.
[15] Zhao S, Takeuchi A, Kimura F, Kajihara Y. Experimental investigation of the anchoring effect of aluminum/amorphous-plastics joints fabricated by injection molded direct joining. Precis Eng 2022;77:320–7. https://doi.org/10.1016/j.precisioneng.2022.06.013.
[16] Wurzbacher S, Gach S, Reisgen U, Hopmann C. Joining of plastic-metal hybrid components by overmoulding of specially designed form-closure elements. Materwiss Werksttech 2021;52:367–78. https://doi.org/10.1002/mawe.202000158.
[17] Byskov-Nielsen J, Boll JV, Holm AH, Højsholt R, Balling P. Ultra-high-strength micro-mechanical interlocking by injection molding into laser-structured surfaces. Int J Adhes Adhes 2010;30:485–8. https://doi.org/10.1016/j.ijadhadh.2010.03.008.
[18] Gebauer J, Fischer M, Lasagni AF, Kühnert I, Klotzbach A. Laser structured surfaces for metal-plastic hybrid joined by injection molding. J Laser Appl 2018;30:032021. https://doi.org/10.2351/1.5036803.
[19] Huang B, Sun L, Li L, Zhang L, Lin Y, Che J. Experimental investigation of the strength of polymer-steel direct adhesion (PSDA) joints with micro-structures ablated by laser. J Mater Process Technol 2017;249:407–14. https://doi.org/10.1016/j.jmatprotec.2017.06.031.
[20] Enami K, Kimura F, Yokoyama K, Murakami T, Kajihara Y. Experimental and simulative investigation of the effects of laser-structured metal surface on metal-polymer direct joining. Precis Eng 2020;62:273–81. https://doi.org/10.1016/j.precisioneng.2019.12.011.
[21] M. Authors, Volume 2: Properties and selection: Nonferrous alloys and Special-Purpose materials, second ed., ASM International, United States of America, n.d..
[22] SABIC Americas. Lexan RESIN 103 - Technical data sheet. 2023.
[23] Ramani K, Moriarty B. Thermoplastic bonding to metals via injection molding for macro-composite manufacture. Polym Eng Sci 1998;38:870–7. https://doi.org/10.1002/pen.10253.

[24] Li X, Liu F, Gong N, Huang P, Yang C. Enhancing the joining strength of injection-molded polymer-metal hybrids by rapid heating and cooling. J Mater Process Technol 2017;249:386–93. https://doi.org/10.1016/j.jmatprotec.2017.06.034.
[25] Li X, Gong N, Yang C, Zeng S, Fu S, Zhang K. Aluminum/polypropylene composites produced through injection molding. J Mater Process Technol 2018;255:635–43. https://doi.org/10.1016/j.jmatprotec.2018.01.008.
[26] Li X, Liu F, Gong N, Yang C, Wang B. Surface topography induced high injection joining strength of polymer-metal composite and fracture mechanism. Compos Struct 2018;184:545–53. https://doi.org/10.1016/j.compstruct.2017.10.020.
[27] Gong N, Wang B, Wang Y, Li X, Lin W, Fu S, Chu X. Effect of metal surface state on injection joining strength of aluminum-rubber composite part. J Manuf Process 2020;49:365–72. https://doi.org/10.1016/j.jmapro.2019.12.006.
[28] Izadi O, Mosaddegh P, Silani M, Dinari M. An experimental study on mechanical properties of a novel hybrid metal–polymer joining technology based on a reaction between isocyanate and hydroxyl groups. J Manuf Process 2017;30:217–25. https://doi.org/10.1016/j.jmapro.2017.09.022.
[29] Bonded joints and Repairs to composite Airframe structures. In: Wang C, Duong C, editors. Damage tolerance and fatigue durability of Scarf joints. Oxford: Academic Press; 2016. p. 72–141.
[30] Grandt A. Introduction to damage tolerance analysis methodology: damage tolerance of Metallic structures: analysis methods and applications. West Conshohocken: ASTM International; 1984.
[31] Yoon SH, Hong CS. Modified end notched flexure specimen for mixed mode interlaminar fracture in laminated composites. Int J Fract 1990;43. https://doi.org/10.1007/BF00018129. R3–R9.
[32] Chaves FJP, da Silva LFM, de Moura MFSF, Dillard DA, Esteves VHC. Fracture Mechanics tests in adhesively bonded joints: a literature review. J Adhes 2014;90:955–92. https://doi.org/10.1080/00218464.2013.859075.
[33] Andre N, Amancio-Filho S. Mechanical integrity and corrosion behavior of metalcomposite hybrid joints produced with Friction Spot Joining. Technischen Universität Hamburg (TUHH); 2020.
[34] American Society for Testing and Materials. Standard test method for apparent shear strength of single-lap-joint adhesively bonded metal specimens by tension loading (Metal-to-Metal) - d1002. 2019.
[35] Dealy JM, Wissbrun KF. Melt rheology and its Role in plastics processing. Springer Netherlands; 1990. https://doi.org/10.1007/978-94-009-2163-4.
[36] Falck RMM. A new additive manufacturing technique for layered metal-composite hybrid structures. Technische Universität Hamburg; 2020.
[37] American Society for testing and materials, standard Practice for statistical analysis of linear or Linearized stress-life (S-N) and Strain-life (ε-N) fatigue data - e739. 2010.
[38] Schijve J, editor. Fatigue of structures and materials. Dordrecht: Springer Netherlands; 2009. https://doi.org/10.1007/978-1-4020-6808-9.
[39] Plaine AH, Suhuddin UFH, Alcântara NG, dos Santos JF. Fatigue behavior of friction spot welds in lap shear specimens of AA5754 and Ti6Al4V alloys. Int J Fatigue 2016;91:149–57. https://doi.org/10.1016/j.ijfatigue.2016.06.005.
[40] Jiang H, Luo T, Li G, Zhang X, Cui J. Fatigue life assessment of electromagnetic riveted carbon fiber reinforce plastic/aluminum alloy lap joints using Weibull distribution. Int J Fatigue 2017;105:180–9. https://doi.org/10.1016/j.ijfatigue.2017.08.026.
[41] Wang F, Bu H, Luo J, Zhang P, Wang L, Zhan X. Influence of different micro-pattern types on interface characteristic and mechanical property of CFRTP/aluminum alloy laser bonding joint. Int J Adv Manuf Technol 2022;120:3543–57. https://doi.org/10.1007/s00170-022-08748-6.
[42] Rodríguez-Vidal E, Sanz C, Lambarri J, Quintana I. Experimental investigation into metal micro-patterning by laser on polymer-metal hybrid joining, vol. 104; 2018. p. 73–82. https://doi.org/10.1016/j.optlastec.2018.02.003.
[43] Christensen R. Analysis of variance, design, and regression: applied statistical methods. New York: CRC Press reprint; 1996.
[44] Choi D-S, Im Y-T. Prediction of shrinkage and warpage in consideration of residual stress in integrated simulation of injection molding. Compos Struct 1999;47:655–65. https://doi.org/10.1016/S0263-8223(00)00045-3.
[45] Lucchetta G, Marinello F, Bariani PF. Aluminum sheet surface roughness correlation with adhesion in polymer metal hybrid overmolding. CIRP Ann Manuf Technol 2011;60:559–62. https://doi.org/10.1016/j.cirp.2011.03.073.
[46] Chang Dae han, rheology in polymer processing. New York: Oxford University Press, Inc.; 2007.
[47] Tanaka Y, Sako T, Hiraoka T, Yamaguchi M, Yamaguchi M. Effect of morphology on shear viscosity for binary blends of polycarbonate and polystyrene. J Appl Polym Sci 2020;137. https://doi.org/10.1002/app.49516.
[48] Bonpain B, Stommel M. Influence of surface roughness on the shear strength of direct injection molded plastic-aluminum hybrid-parts. Int J Adhes Adhes 2018;82:290–8. https://doi.org/10.1016/j.ijadhadh.2018.02.003.
[49] Li X, Wang B, Xu D, Wang B, Dong W, Li M. Super-high bonding strength of polyphenylene sulfide-aluminum alloy composite structure achieved by facile molding methods. Compos B Eng 2021;224. https://doi.org/10.1016/j.compositesb.2021.109204.
[50] Wang S, Kimura F, Zhao S, Yamaguchi E, Ito Y, Kajihara Y. Influence of fluidity improver on metal-polymer direct joining via injection molding. Precis Eng 2021;72:620–6. https://doi.org/10.1016/j.precisioneng.2021.07.001.
[51] Kimura F, Yamaguchi E, Horie N, Suzuki G, Kajihara Y. Formation of boehmite crystals on microblasted aluminum surface to enhance performance of metal–polymer direct joining. Mater Lett 2020;260:126963. https://doi.org/10.1016/j.matlet.2019.126963.
[52] Kadoya S, Kimura F, Kajihara Y. PBT–anodized aluminum alloy direct joining: characteristic injection speed dependence of injected polymer replicated into nanostructures. Polym Test 2019;75:127–32. https://doi.org/10.1016/j.polymertesting.2019.02.006.
[53] Yin S, Xie Y, Li R, Zhang J, Zhou T. Polymer-metal hybrid material with an Ultra-high interface strength based on mechanical interlocking via Nanopores produced by Electrochemistry. Ind Eng Chem Res 2020;59:12409–20. https://doi.org/10.1021/acs.iecr.0c01304.
[54] Kleffel T, Drummer D. Investigating the suitability of roughness parameters to assess the bond strength of polymer-metal hybrid structures with mechanical adhesion. Compos B Eng 2017;117:20–5. https://doi.org/10.1016/j.compositesb.2017.02.042.
[55] Du M, Dong W, Li X, Wang L, Wang B, Tang B. Effect of surface topography on injection joining Ti alloy for improved bonding strength of metal-polymer. Surf Coat Technol 2022;433. https://doi.org/10.1016/j.surfcoat.2022.128132.
[56] Verma S, Yang CK, Lin CH, Jeng JY. Additive manufacturing of lattice structures for high strength mechanical interlocking of metal and resin during injection molding. Addit Manuf 2022;49. https://doi.org/10.1016/j.addma.2021.102463.
[57] Fabrin PA, Hoikkanen ME, Vuorinen JE. Adhesion of thermoplastic elastomer on surface treated aluminum by injection molding. Polym Eng Sci 2007;47:1187–91. https://doi.org/10.1002/pen.20801.
[58] Kimura F, Kadoya S, Kajihara Y. Effects of molding conditions on injection molded direct joining under various surface fine-structuring. Int J Adv Manuf Technol 2019;101:2703–12. https://doi.org/10.1007/s00170-018-3154-8.
[59] Kimura F, Kadoya S, Kajihara Y. Effects of molding conditions on injection molded direct joining using a metal with nano-structured surface. Precis Eng 2016;45:203–8. https://doi.org/10.1016/j.precisioneng.2016.02.013.
[60] Yeh RY, Hsu RQ. Improving the adhesion of plastic/metal direct bonding by injection moulding using surface modifications. Advances in Materials and Processing Technologies 2016;2:21–30. https://doi.org/10.1080/2374068X.2016.1147765.
[61] Zhao S, Kimura F, Yamaguchi E, Horie N, Kajihara Y. Manufacturing aluminum/polybutylene terephthalate direct joints by using hot water–treated aluminum via injection molding. Int J Adv Manuf Technol 2020;107:4637–44. https://doi.org/10.1007/s00170-020-05364-0.
[62] Boerio FJ, Shah P. Adhesion of injection molded PVC to steel substrates. J Adhes 2005;81:645–75. https://doi.org/10.1080/00218460590954656.
[63] Honkanen M, Hoikkanen M, Vippola M, Vuorinen J, Lepistö T. Metal-plastic adhesion in injection-molded hybrids. J Adhes Sci Technol 2009;23:1747–61. https://doi.org/10.1163/016942409X12489445844435.
[64] Hoikkanen M, Honkanen M, Vippola M, Lepistö T, Vuorinen J. Effect of silane treatment parameters on the silane layer formation and bonding to thermoplastic urethane. Prog Org Coat 2011;72:716–23. https://doi.org/10.1016/j.porgcoat.2011.08.002.
[65] Hoikkanen M, Honkanen M, Frisk L, Vippola M, Lepistö T, Vuorinen J. Metal-thermoplastic urethane hybrids in environmental exposure. Int J Adhes Adhes 2012;35:21–6. https://doi.org/10.1016/j.ijadhadh.2012.01.024.
[66] Liu FC, Dong P, Lu W, Sun K. On formation of Al–O–C bonds at aluminum/polyamide joint interface. Appl Surf Sci 2019;466:202–9. https://doi.org/10.1016/j.apsusc.2018.10.024.
[67] Goushegir SM, Scharnagl N, dos Santos JF, Amancio-Filho ST. XPS analysis of the interface between AA2024-T3/CF-PPS friction spot joints. In: Surface and interface analysis. John Wiley and Sons Ltd; 2016. p. 706–11. https://doi.org/10.1002/sia.5816.
[68] Schijve J, Campoli G, Monaco A. Fatigue of structures and secondary bending in structural elements. Int J Fatigue 2009;31:1111–23. https://doi.org/10.1016/j.ijfatigue.2009.01.009.
[69] Abibe AB, Amancio-Filho ST, dos Santos JF, Hage E. Mechanical and failure behaviour of hybrid polymer–metal staked joints. Mater Des 2013;46:338–47. https://doi.org/10.1016/j.matdes.2012.10.043.
[70] Goushegir SM, dos Santos JF, Amancio-Filho ST. Fatigue performance of metal–composite friction spot joints. Materials 2021;14:4516. https://doi.org/10.3390/ma14164516.
[71] Fang QZ, Wang TJ, Li HM. Overload-induced retardation of fatigue crack growth in polycarbonate. Int J Fatigue 2008;30:1419–29. https://doi.org/10.1016/j.ijfatigue.2007.10.005.
[72] Takemori MT. Fatigue fracture of polycarbonate. Polym Eng Sci 1982;22:937–45.
[73] Banasiak DH, Grandt AF, Montulli LT. Fatigue crack retardation in polycarbonate. J Appl Polym Sci 1977;21:1297–309. https://doi.org/10.1002/app.1977.070210513.
[74] Banasiak DH, Grandt AF, Montulli LT. Fatigue crack retardation in polycarbonate. J Appl Polym Sci 1977;21:1297–309.
[75] Schmidt H-J, Schmidt-Brandecker B. Effect of fatigue and damage tolerance material properties on the efficiency of aircraft structures. In: ICAA13 Pittsburgh. Cham: Springer International Publishing; 2012. p. 461–70. https://doi.org/10.1007/978-3-319-48761-8_67.
[76] Wimberger-Friedl R. Molecular orientation induced by cooling stresses. Birefringence in polycarbonate: III. Constrained quench and injection molding. J Polym Sci B Polym Phys 1994;32:595–605. https://doi.org/10.1002/polb.1994.090320401.
[77] Dar UA, Xu YJ, Zakir SM, Saeed M-U. The effect of injection molding process parameters on mechanical and fracture behavior of polycarbonate polymer. J Appl Polym Sci 2017;134. https://doi.org/10.1002/app.44474.

[78] Pham HT, Bosnyak CP, Sehanobish K. Residual stresses in injection molded polycarbonate rectangular bars. Polym Eng Sci 1993;33:1634–43. https://doi.org/10.1002/pen.760332408.
[79] Haghighi-Yazdi M, Tang JKY, Lee-Sullivan P. Moisture uptake of a polycarbonate blend exposed to hygrothermal aging. Polym Degrad Stab 2011;96:1858–65. https://doi.org/10.1016/j.polymdegradstab.2011.07.007.
[80] Borba NZ, dos Santos JF, Amancio-Filho ST. Hydrothermal aging of friction riveted thermoplastic composite joints for aircraft applications. Compos Struct 2021;255:112871. https://doi.org/10.1016/j.compstruct.2020.112871.